

Absence of amorphous phase in high power femtosecond laser-ablated silicon

Matthew S. Rogers,¹ Costas P. Grigoropoulos,¹ Andrew M. Minor,² and Samuel S. Mao^{1,3,a)}

¹*Department of Mechanical Engineering, University of California at Berkeley, Berkeley, California 94720, USA*

²*Department of Materials Science and Engineering, University of California at Berkeley, Berkeley, California 94720, USA and National Center for Electron Microscopy, Lawrence Berkeley National Laboratory, Berkeley, California 94720, USA*

³*Advanced Energy Technologies Department, Lawrence Berkeley National Laboratory, Berkeley, California 94720, USA*

(Received 20 September 2008; accepted 25 November 2008; published online 8 January 2009)

As femtosecond lasers emerge as viable tools for advanced microscale materials processing, it becomes increasingly important to understand the characteristics of materials resulting from femtosecond laser microablation or micromachining. We conducted transmission electron microscopy experiments to investigate crater structures in silicon produced by repetitive high power femtosecond laser ablation. Comparable experiments of nanosecond laser ablation of silicon were also performed. We found that an amorphous silicon layer that is typically produced in nanosecond laser ablation is absent when the material is irradiated by high power femtosecond laser pulses. Instead, only a defective single crystalline layer was observed in the high power femtosecond laser-ablated silicon crater. Possible mechanisms underlying the formation of the defective single crystalline phase are discussed. © 2009 American Institute of Physics. [DOI: 10.1063/1.3052693]

Lasers that can produce photon pulses with duration in the femtosecond regime opened up new frontiers in materials processing.¹ Applications such as machining of microscale and nanoscale features and deposition of nanostructured films depend upon an understanding of the complex laser-material interaction processes resulting from high power femtosecond laser irradiation. Single crystal silicon has been a model system for studying the basic characteristics of laser-ablated materials, in connection to many electronic applications. Previous materials research efforts on repetitive femtosecond laser interaction with silicon have been mostly based on either using low (<0.1 J/cm²) or moderate (up to 3.0 J/cm²) laser fluences,^{2,3} as well as using a large number of pulses in a reactive background gas.⁴ It was found that a thin amorphous silicon layer can be created after laser ablation when the fluences are not much above the ablation threshold for forming a crater on laser-irradiated silicon surface.⁵ From the point of view of femtosecond laser micromachining or deposition, desirable fluence for repetitive laser irradiation would be well into the ablation regime. In view of the significance of the respective applications as well as the very limited literature reports on the structural characteristics of high power laser-ablated materials, we have focused our effort on examining a high laser fluence regime (~ 28 J/cm²).

Laser-machined lines were generated in a (001) Si wafer using a frequency tripled Ti:sapphire femtosecond laser (Spectra-Physics) with a wavelength of 266 nm and a pulse duration of approximately 120 fs. The same experiments were conducted using a frequency quadrupled neodymium-doped yttrium aluminum garnet (Nd:YAG) laser (Coherent) with a wavelength of 266 nm and a pulse duration of 4 ns. Both lasers were operated at a 10 Hz repetition rate. The

Nd:YAG laser-ablated sample was scanned at 100 μ m/s, and the Ti:sapphire sample was scanned at 20 μ m/s. Different scan rates were used as femtosecond and nanosecond laser pulses have different spot sizes. The scan rate does not affect comparing femtosecond and nanosecond laser ablated craters, as long as the spots under study receive multiple laser shots. After laser ablation, the silicon sample was cut into thin slices using a diamond saw, thinned to optical transparency by dimpling, attached to a transmission electron microscopy (TEM) grid, and then thinned to electron transparency using an Ar ion mill.

The ablation crater size was measured optically using a white light interferometer. An energy of 92 μ J/pulse and a crater size of 20 μ m was used for femtosecond laser ablation, while a 547 μ J/pulse energy and 50 μ m crater was used for nanosecond laser ablation. These conditions correspond to a laser fluence of approximately 28 J/cm² for both cases. The prepared samples were investigated using a JEOL 3010 TEM, and representative TEM images are presented in this report. Due to the relatively large size of the ablation craters, multiple low magnification images were necessary to image the crater.

For the nanosecond laser-ablated crater, the boxed image in Fig. 1 was patched together from 19 separate images. For clarity, a representative schematic is also shown in Fig. 1. Inspection of the nanosecond laser created crater revealed three separate regimes. The top regime [Fig. 1(a)] was inspected using selected area electron diffraction (SAED) and is composed of primarily amorphous silicon. The thickness of this regime was measured at 100 locations around the crater and the average thickness was about 1 μ m with a standard deviation of 300 nm. The region in Fig. 1(b) is a fundamentally different regime than the region in Fig. 1(a). The SAED pattern from the region in Fig. 1(b) reveals that the original crystallinity of the Si wafer was preserved in this regime. Bright field imaging shows that there is a high den-

^{a)}Electronic addresses: ssmao@me.berkeley.edu and ssmao@lbl.gov.

Report Documentation Page

Form Approved
OMB No. 0704-0188

Public reporting burden for the collection of information is estimated to average 1 hour per response, including the time for reviewing instructions, searching existing data sources, gathering and maintaining the data needed, and completing and reviewing the collection of information. Send comments regarding this burden estimate or any other aspect of this collection of information, including suggestions for reducing this burden, to Washington Headquarters Services, Directorate for Information Operations and Reports, 1215 Jefferson Davis Highway, Suite 1204, Arlington VA 22202-4302. Respondents should be aware that notwithstanding any other provision of law, no person shall be subject to a penalty for failing to comply with a collection of information if it does not display a currently valid OMB control number.

1. REPORT DATE 2009	2. REPORT TYPE	3. DATES COVERED 00-00-2009 to 00-00-2009	
4. TITLE AND SUBTITLE Absence of amorphous phase in high power femtosecond laser-ablated silicon		5a. CONTRACT NUMBER W911NF-06-1-0446	
		5b. GRANT NUMBER	
		5c. PROGRAM ELEMENT NUMBER	
6. AUTHOR(S)		5d. PROJECT NUMBER	
		5e. TASK NUMBER	
		5f. WORK UNIT NUMBER	
7. PERFORMING ORGANIZATION NAME(S) AND ADDRESS(ES) Department of Mechanical Engineering, University of California at Berkeley, Berkeley, CA, 94720		8. PERFORMING ORGANIZATION REPORT NUMBER ; 50531.9	
9. SPONSORING/MONITORING AGENCY NAME(S) AND ADDRESS(ES) U.S. Army Research Office, P.O. Box 12211, Research Triangle Park, NC, 27709-2211		10. SPONSOR/MONITOR'S ACRONYM(S)	
		11. SPONSOR/MONITOR'S REPORT NUMBER(S) 50531.9	
12. DISTRIBUTION/AVAILABILITY STATEMENT Approved for public release; distribution unlimited			
13. SUPPLEMENTARY NOTES			
14. ABSTRACT			
15. SUBJECT TERMS			
16. SECURITY CLASSIFICATION OF:			17. LIMITATION OF ABSTRACT
a. REPORT unclassified	b. ABSTRACT unclassified	c. THIS PAGE unclassified	Same as Report (SAR)
			18. NUMBER OF PAGES 4
			19a. NAME OF RESPONSIBLE PERSON

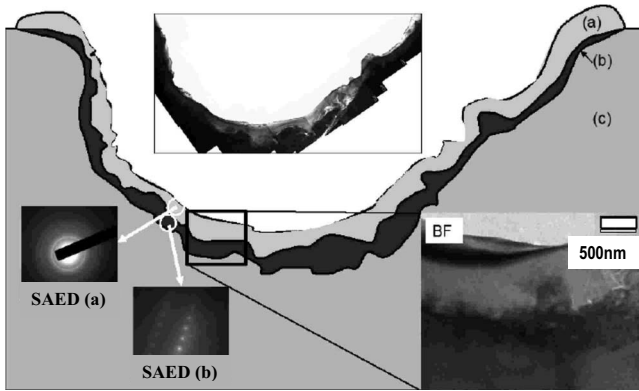


FIG. 1. Cross-sectional TEM image from the nanosecond laser-ablated silicon. A schematic is shown displaying the three regimes present after ablation. (a) is an amorphous regime, (b) is a single crystal with a high defect density, and (c) is the underlying undamaged single crystal Si substrate. A bright field image is shown of the three regimes and a SAED pattern is shown for regions (a) and (b).

sity of defects in this region. The average thickness was found to be 600 nm, with a standard deviation of 200 nm. The region in Fig. 1(c) is the undamaged, unaffected silicon. The thin dark lines evident in region 3 are bend contours.

High magnification was used to directly image the amorphous regime in Fig. 1(a); the results are shown in Fig. 2(a). Figure 2(b) shows an image of a converged electron beam with a spot size of approximately 10 nm. This nanobeam is utilized for measuring electron diffraction of the amorphous regime; the corresponding nanobeam electron diffraction (NBED) pattern is given in Fig. 2(c). The pattern is mostly amorphous with individual bright spots corresponding to diffraction from very small crystallites. The change from a crystalline to an amorphous phase is indicative of a phase change, as severe undercooling of silicon melt coupled with a high cooling rate can result in amorphization of liquid silicon after laser ablation.⁶

The TEM results for femtosecond laser-ablated silicon are given in Fig. 3, where a schematic is also used to illustrate different observed regimes. In the case of the high power femtosecond laser-created crater, no amorphous regime was found. The area near the surface was examined in an effort to identify an amorphous regime similar to that observed in Figs. 1(a) and 2 using high magnification bright field imaging (SAED) and NBED investigations. However, no such regime could be identified. The bright field image in Fig. 3 clearly shows only two regimes. The highly defective, yet crystalline regime, exists at the surface of the crater as shown in Fig. 3(b), and below lays the undisturbed Si substrate, as shown in Fig. 3(c). The different SAED patterns shown for Figs. 3(b) and 1(b) are caused by investigation under different TEM tilt conditions, and therefore correspond

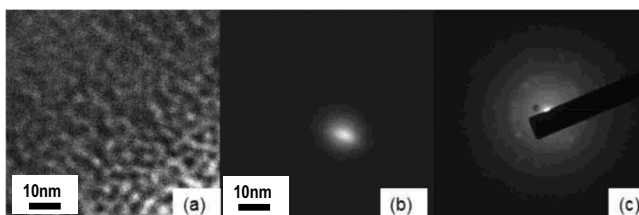


FIG. 2. (a) Bright field image of the grains in the amorphous regime. (b) Image of the NBED spot. (c) Corresponding NBED pattern.

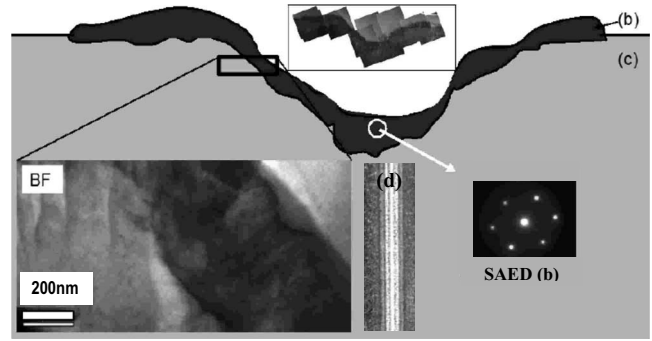


FIG. 3. Cross-sectional TEM image from the femtosecond laser-ablated silicon. A schematic is shown displaying the two regimes present after ablation. (b) is a single crystal with a high defect density and (c) is the underlying undamaged single crystal Si substrate. A bright field image is shown of the two regimes and a SAED pattern is shown for region (b). The insert (d) is an optical dark field image of a section of fs laser produced line.

to different zone axes. Both samples are crystalline in this regime, but contain a high defect density. The thickness of the defect regime for the femtosecond laser ablation case was measured to be 400 nm thick on average, with a standard deviation of 200 nm.

The resolidification of melted silicon during laser annealing has been extensively studied. Silicon melt regrowth has been observed to occur as amorphous, polycrystalline, and single crystalline. A thin liquid melt may resolidify epitaxially under proper conditions, as determined by the interface response function of the material, which depends on the amount of supercooling and the resolidification front velocity, as well as a host of material properties.^{7,8} As the cross-sectional TEM images in Fig. 4 reveal, melting and epitaxial resolidification may have occurred following high power femtosecond laser irradiation of silicon, yielding defective crystal growth. The same defective crystalline layer appears in the nanosecond laser-ablated crater as well [Fig. 1(b)] but in this case an amorphous phase exists above the defective region [Fig. 1(a)].

Alternatively, the observed highly defective crystalline region for both high power femtosecond and nanosecond laser-ablated silicon is indicative of large mechanical stresses during ablation.⁹ Peak pressures in the GPa range have been predicted to occur during laser ablation.¹⁰ Molecular-dynamics simulations have shown that dislocations may be caused by the large thermomechanical stresses that occur during ablation.¹¹ Thus dislocation formation can occur via

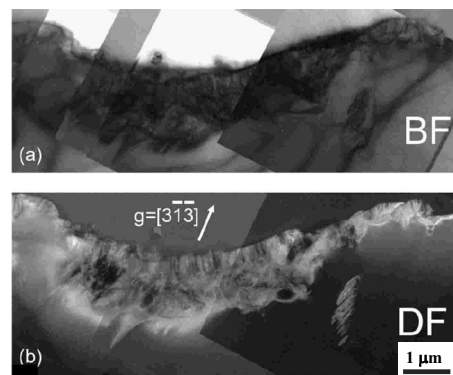


FIG. 4. Cross-sectional TEM image from the fs laser-ablated silicon. (a) Bright field and (b) a dark field image in the $[3\bar{1}\bar{3}]$ dark field condition.

laser-induced shockwave interaction and throughout the ablation process when a thermomechanical stress is built up. Consequently, the defective single crystalline regime may form due to large thermomechanical stress. A shock wave propagating into the laser-ablated silicon also yields a large defect density in the otherwise perfect silicon crystal. These defects can grow into the hot but unmelted silicon, exhibiting a metal-like flow. Dislocations have been observed to flow freely in silicon at temperatures above 725 K,¹² as well as at room temperature under very high pressures.¹³

It is also interesting to observe that the crater rim (Fig. 3) of femtosecond laser-ablated silicon is defective single crystalline, as compared to amorphous crater rim (Fig. 1) that resulted from nanosecond laser ablation. Previous *in situ* nanoindentation TEM studies observed metal-like extrusions resulting from plastic deformation in the absence of a phase transformation.¹⁴ The raised rims around the nanoindented crater exist in a defective single crystalline phase. Thus it is possible to form a raised crater rim in the absence of liquid resolidification simply by the action of a metal-like flow of dislocations in silicon, which is under high temperature and extreme pressure. A slight change ($<2^\circ$) was observed in the zone axis orientation between the unaffected bulk single crystalline silicon and the defective single crystal regime, which can be explained as the result of the strain during laser ablation. This scenario does not rule out melting in the case of femtosecond laser ablation of silicon, but implies that the melt is perhaps more efficiently removed from the crater than in the case of nanosecond laser ablation, wherein a large amorphous regime is observed.

In summary, TEM investigations of high power femtosecond and nanosecond laser-ablated silicon are performed. A cross-sectional view of the nanosecond case revealed an amorphous surface regime of approximately 1 μm in depth, followed by a 600 nm defective crystalline regime. The high power femtosecond laser ablation crater did not show any amorphization, but a 400 nm defect crystalline layer was created. This defective crystalline layer can result from a laser-induced stress mechanism due to shockwave or thermomechanical deformation. The missing amorphous regime in

the case of high power femtosecond laser-ablated silicon as compared to nanosecond laser ablation is indicative of less residual energy left in the substrate after ablation. We expect that this current study would generate interests in modeling structural evolution under laser ablation, which will yield more insight into the dominant mechanism for the formation of a defective single crystalline layer in the absence of the amorphous phase.

This research has been supported by the U.S. Department of Defense, Army Research Office Contract No. W911NF-06-1-0446, under Multidisciplinary University Research Initiative. Research performed at the National Center for Electron Microscopy, Lawrence Berkeley National Laboratory, was supported by the Scientific User Facilities Division of the Office of Basic Energy Sciences, Office of Science, U.S. Department of Energy under Contract No. DE-AC02-05CH11231.

¹S. S. Mao, F. Quéré, S. Guizard, X. Mao, R. E. Russo, G. Petite, and P. Martin, *Appl. Phys. A: Mater. Sci. Process.* **79**, 1695 (2004).

²J. Jia, M. Li, and C. Thompson, *Appl. Phys. Lett.* **84**, 3205 (2004).

³Y. Izawa, Y. Izawa, Y. Setsuhara, M. Hashida, M. Fujita, R. Sasaki, H. Nagai, and M. Yoshida, *Appl. Phys. Lett.* **90**, 044107 (2007).

⁴T. Her, R. Finlay, S. Deliwala, and E. Mazur, *Appl. Phys. Lett.* **73**, 1673 (1998).

⁵A. Cavalleri, K. Sokoloski-Tinten, J. Bialkowski, M. Schreiner, and D. Linde, *J. Appl. Phys.* **85**, 3301 (1999).

⁶Y. Shao, F. Spaepen, and D. Turnbull, *Metall. Mater. Trans. A* **29A**, 1835 (1998).

⁷C. Grigoropoulos, M. Rogers, S. Ko, A. Golovin, and B. Matkowsky, *Phys. Rev. B* **73**, 184125 (2006).

⁸M. Thompson, J. Mayer, A. Cullis, H. Webber, N. Chew, J. Poate, and D. Jacobson, *Phys. Rev. Lett.* **50**, 896 (1983).

⁹B. Chalmers, *Principles of Resolidification* (Wiley, New York, 1964).

¹⁰K. Sokoloski-Tinten, J. Bialkowski, A. Cavalleri, D. von der Linde, A. Oparin, J. Meyer-ter-Vehn, and S. Anisimov, *Phys. Rev. Lett.* **81**, 224 (1998).

¹¹D. Bouilly, D. Perez, and L. Lewis, *Phys. Rev. B* **76**, 184119 (2007).

¹²A. Kelly and N. Macmillan, *Strong Solids* (Clarendon, Oxford, 1986).

¹³H. Saka, A. Shimatani, M. Sugauma, and Suprijadi, *Philos. Mag. A* **82**, 1971 (2002).

¹⁴A. Minor, E. Lilleodden, M. Jin, E. Stach, D. Chrzan, and J. Morris, Jr., *Philos. Mag. A* **85**, 323 (2005).